Final manuscript : *Physics of Fluids*, Vol. 7, no. 9, 2271-2279, Sept. 1995.

Laser Light Scattering By Shock Waves

J. Panda*
The University of Toledo
Toledo, Ohio

G. Adamovsky
NASA Lewis Research Center
Cleveland, Ohio

ABSTRACT

Scattering of coherent light as it propagates parallel to a shock wave, formed in front of a bluff cylindrical body placed in a supersonic stream, is studied experimentally and numerically. Two incident optical fields are considered. First, a large diameter collimated beam is allowed to pass through the shock containing flow. The light intensity distribution in the resultant shadowgraph image, measured by a low light CCD camera, shows well-defined fringes upstream and downstream of the shadow cast by the shock. In the second situation, a narrow laser beam is brought to a grazing incidence on the shock and the scattered light, which appears as a diverging sheet from the point of interaction, is visualized and measured on a screen placed normal to the laser path. Experiments are conducted on shocks formed at various free-stream Mach numbers, M, and total pressures, P_0. It is found that the widths of the shock shadows in a shadowgraph image become independent of M and P_0 when plotted against the jump in the refractive index, Δn, created across the shock. The total scattered light measured from the narrow laser beam and shock interaction also follows the same trend. In the numerical part of the study, the shock is assumed to be a `phase object', which introduces phase difference between the upstream and downstream propagating parts of the light disturbances. For a given shape and Δn of the bow shock the phase and amplitude modulations are first calculated by ray tracing. The wave front is then propagated to the screen using the Fresnel diffraction equation. The calculated intensity distribution, for both of the incident optical fields, shows good agreement with the experimental data.

PACS NO. 51.70.+f; 42.25.Fx; 47.40.Nm; 43.28.+h

I. INTRODUCTION

A significant change of gas density across a shock is accompanied by a change in the refractive index. Upstream of the shock is a region of lower and, downstream is a region of higher refractive index. A large deflection of light rays across this change in refractive index makes the shock easily visible in Schlieren and shadowgraph images. The phenomenon is usually explained with the laws of geometrical optics (Merzkirch[1], page 115). However, a shock is also expected to cause light diffraction, as the extremely small thickness effectively makes it a sharp interface between the optically different upstream and downstream regions. The objective of the present work is to explore the light diffraction effects caused by a shock wave. This paper presents extensive experimental evidence and a numerical calculation based on the Huygens-Fresnel principle[2] to explain this phenomenon.

Two different optical conditions, both of which involve significant diffraction effects as laser light propagates parallel to a shock surface, are considered. The first one is the well-known shadowgraph situation, where a large diameter collimated laser beam is allowed to pass through the shock containing region and the shadowgraph image formed on a screen is studied.

* Resident Research Associate, NASA Lewis Research Center, Cleveland, OH 44135.
Corresponding author. (voice): 216-433-8891, (fax): 216-433-5802, (email): panda@yaz.lerc.nasa.gov

The second is somewhat unknown and was first reported by Panda[3,4]. It involves a narrow laser beam brought to a grazing incidence on a shock surface. In this situation a thin diverging light sheet is found to appear from the point of interaction. The visible divergence angle of the light sheet is very large, up to ±10° depending upon the shock strength, and the light appears both upstream and downstream of the shock. When a screen is placed normal to the laser path, the cross-section of the sheet appears as a long, bright streak. The scattered light is found to disappear at all other incidence angles when the laser beam pierces the shock. The optical phenomenon is also believed to appear primarily due to diffraction of laser light by shock waves; however, sufficient evidence to determine the exact nature of the phenomenon was absent. It has been demonstrated that the phenomenon can be used as the basis of a novel shock detection technique[3,5] which is convenient in detecting unsteady shock motion. A major motivation of this work is to determine the effects of various fluid dynamic and optical parameters on the scattered light, as well as to establish the physics behind the phenomenon.

Evidence of diffraction fringes in the shadow image of a shock can be found in many earlier experiments[6,7]. Pfeifer *et al*[8]. have shown that for a plane shock, the zeroth diffraction order is a minimum, which appears in the shadowgraph to form the dark band. Merzkirch[1] also discusses that, when the incident light waves propagate parallel to the surface of the shock the major contribution to the formation of a shadow is light diffraction (see discussion in page 133). However, all of these discussions are very limited in scope and frequently the diffraction effects are overlooked. Wide angle scattering of a narrow beam of light by conducting cylinders has been reported earlier in the literature (see Langois *et al*[9].). However, the present problem involving shock waves is very different. Optical properties of the scattered light such as the intensity distribution, fringe spacing, and the effects of various fluid dynamic parameters were not studied for the diffraction effects caused by a shock wave.

In the experimental part of this study a steady bow shock, formed ahead of a bluff cylinder placed in a supersonic free-stream, is used to study such effects. Light intensity distributions for both the wide angle scattering from a narrow beam and diffraction fringes in shadowgraph images are measured for various free-stream Mach numbers and total pressures. In the numerical part of this study, the phenomena are modeled as due to the phase difference between the light waves travelling upstream and downstream of the shock. The 2-dimensional analysis assumes that the incidence disturbance field is made of plane and parallel waves to model the shadowgraph image and a Gaussian strip to model the narrow laser beam and shock wave interaction. The diffraction patterns are calculated and presented after describing the experimental results. Finally, the similarities and differences between the two situations and various other parameters that may affect the diffraction phenomena are discussed in the conclusion.

II. EXPERIMENTAL FACILITY

The experiments were conducted in a continuous, 127mm X 127mm supersonic wind tunnel at the NASA Lewis Research Center. Details of the tunnel can be found elsewhere[10]. In brief, the tunnel is supplied by compressed air which is discharged into a low vacuum altitude exhaust system. The free-stream Mach number can be varied from 1.5 to 3.0 by changing the nozzle contour. The free-stream total pressure, P_0, also can be varied independently from 134 KPa to 375 KPa. The total temperature of the supplied air is the same as that of the ambient air (294° Kelvin). For the present experiment the test section was equipped with two scratch free Plexiglas windows, each 25.4mm thick. The cylindrical bluff body used to produce a bow shock was mounted edge on with its axis along the flow direction. It was 12.7mm in diameter and was mounted on a sting at the center of the tunnel.

The experiments were conducted at three different free-stream Mach numbers: 1.5, 2.0 and 2.5, and five different free-stream total pressures: 375, 306, 237, 168 and 134 KPa. For the highest Mach number of 2.5 the tunnel could not be started at the lowest total pressure of 134 KPa, and for the lowest Mach number of 1.5 operations were limited to a maximum P_0 of 237 KPa by the maximum allowable mass flux of air supplied to the tunnel.

A 4 mW, random polarization, He-Ne Laser (632.8 nm wavelength) was used as the light source for all experiments. A polarizer, placed in front of the laser was used to change incident beam polarization, and a combination of the polarizer and a neutral density filter was used to cut down the laser power when needed.

The scattered light patterns were visualized on a semi-transparent screen (similar to a ground glass) placed normal to the laser path. The images on the screen were photographed using a cooled CCD camera which provided

quantitative information of the light intensity distribution on the screen. The 12-bit, 576 X 384 pixel camera has a separate refrigeration unit to cool the camera head to -45° Celsius; thereby dropping the dark current significantly. This low noise feature makes the camera useful for measuring low levels of light. The camera has its own controller which, in turn, is interfaced with a 486DX Personal Computer (PC). Images obtained by the CCD camera were stored in the PC and are post-processed to obtain quantitative information. Various Nikon lenses were used on the camera head to expose a wide range of area on the screen.

A laser shadowgraph system was used to obtain a large diameter collimated beam (figure 1). The narrow beam from the He-Ne laser was allowed to pass through a beam expander (made up of a microscope objective, a 25 micron spatial filter and a 300mm focal length lens) and was allowed to pass through the test section. The shadowgraph image formed on the semi-transparent screen placed on the other side of the test section was photographed either by the CCD camera or by a 35mm camera.

III. EXPERIMENTAL RESULTS

Figure 2 shows shadowgraph images of the bow shock formed in front of the bluff body for two different free-stream Mach numbers. For all figures presented in this paper, flow is from left to right. The bow shock is found to become more curved and to move closer to the bluff cylinder as the free-stream Mach number is increased. However, for a fixed M, as P_0 is changed the shock shape and its location are not affected.

A steady shock is essential to achieve the experimental goal. To check the shock steadiness, video recordings of the shadowgraph images were obtained by a separate light intensified CCD camera that can be gated to a fast shutter speed of 20 nano-seconds. A frame by frame analysis showed that the shock was extremely stationary up to $M \leq 2.5$, above which it meandered at a very low frequency, perhaps due to the proximity to the bluff body.

A. Diffraction effects in shadowgraph image of shock

The diffraction effects are not visible in the 35mm photographs of figure 2. To highlight the detail of the shock shadow a small region around the tip of the bow shock along the centerline of the cylindrical body was photographed using the low light CCD camera. Two different images were taken: one without the any airflow, `no flow' image, and a second one with the flow on. Subsequently, the `no flow' image was subtracted from the `flow' image to determine the changes caused by the shock. The processed data clearly show the dark shadow cast by the shock and clear fringes upstream and downstream of the shock. Figures 3(a) and (b) show two such processed images of the bow shock in M = 1.5 free-stream at two different free-stream total pressures. The screen, from which the shadowgraph images were photographed, was placed 685 mm away from the shock location. The dark band representing the shadow of the shock appears very thick due to a magnification of ~8 from figure 2.

A special problem encountered with the laser shadowgraph system is the speckle noise produced by small dust particles on the wind tunnel windows. This random optical noise is easily visible in figures 3(a) and (b). To cancel out the background noise the light intensity data was averaged over a transverse band of 30 pixels. The intensity values presented in figure 3(c) are also normalized by the average intensity of the `no flow' image. The resultant intensity distribution shows that the first fringe downstream of the central dark band is always the brightest. Both downstream and upstream fringes are indicative of light diffraction, whereas some of the extra light in the downstream fringes can also be interpreted from geometrical optics as due to refractive bending of light.

It is found that the width of the central dark band and the intensity modulation in the fringes depend on the free-stream total pressure P_0 and Mach number M. For a fixed M, the light patterns become weaker as P_0 is decreased. This is clearly visible from the two different P_0 cases shown in figure 3. It is possible to simplify this dependency by analyzing the fluid dynamic and the optical properties of the shock. Table I presents such properties calculated for the tip region of the bow shock. Since, the shock is normal to the flow direction at this location, flow properties downstream of the shock are obtained by applying the normal shock relations. The refractive indices (n) are calculated assuming ideal gas behavior, and by applying the Gladstone-Dale relationship[1]: $n-1 = C\rho$, where ρ is the local density of air and C is the Gladstone-Dale constant ($C = 2.25 \times 10^{-4}$ m^3/Kg used for the laser wavelength). Data in Table I show that as P_0 is decreased keeping M constant, the air density, both upstream and downstream of the shock, decreases. The refractive indices also follow the same trend. The last column of Table I show that the net

difference of the index of refraction, Δn, between the upstream and downstream regions decreases with a decrease in P_0. The dependence on M for a fixed P_0, however, is not straightforward as the density change across a shock is a non-linear function of M. Nonetheless, it is found that the jump in the refractive index across a shock is the single most important parameter that controls the shadow formation in the shadowgraph images. This is shown in figure 4 where the width of the central dark band, representing the shadow of the shock, is plotted against Δn. The data points are obtained from shadowgraph images on a screen placed at a fixed distance of 216mm away from the shock and for different M and P_0 conditions. The normalized light intensity distributions, similar to figure 3(c), were obtained from each image and the thickness of the shadow is measured as the width between the unit intensity points of the trough representing the shock shadow. The refractive index jump, Δn, is obtained from table I. Figure 4 shows that the shadow width increases with Δn and is independent of M and P_0. The implication of this result is that the only way any change in the fluid dynamic parameters affects the optical scattering is by changing the optical property of the medium that is the net jump in the refractive index across a shock. Somewhat similar behavior is also observed when a narrow laser beam is used to study the shock laser interaction. This is discussed next.

B. Narrow laser beam and shock interaction

Figure 5 shows a schematic of the arrangement to measure the scattered light produced from such an interaction. When the narrow laser beam is brought to a grazing incidence on the bow shock, the scattered light appears as a diverging sheet from the main laser beam. For all data presented in this paper, the laser beam is made to touch the tip region of the bow shock. The light patterns, as photographed from a screen placed normal to the laser path and 480mm away from the shock, are shown in Figure 6. The long streaks, extending far upstream and downstream from the shock, are aligned with the flow direction. If the laser beam is moved to touch any other part of the bow shock, the streaks are found to become inclined along the local normal to the shock surface. Various other features including the directional dependence of the scattered light have been discussed earlier[3,4]. The scale at the bottom of the figure shows the angular spread (θ) of the scattered light. The angular spread angle is defined as,

$$\theta = \tan^{-1}\left(\frac{\text{Distance on screen from center of the laser spot}}{\text{shock to screen distance}}\right), \qquad \textbf{(1)}$$

and is also shown in the schematic of figure 5. The wide angle light streaks are definite evidence of diffraction effect. Figures 6(b), (c) and (d) correspond to a decreasing P_o while the free-stream Mach number was kept constant. Clearly, the phenomenon weakens progressively as P_o is decreased. Note that the laser beam, whose cross-section is seen as a bright central spot, splits into two parts after touching the shock.

Quantitative measurement of the light intensity distribution in the long streaks was not straightforward as the intensity varied by many orders of magnitude from the center of the laser beam to the visible end of the streaks. To satisfy the conflicting requirements of avoiding saturation from the intense main laser beam and having sufficient exposure to capture the weak tail, data were obtained in two steps. At first, the laser power is reduced considerably by placing a neutral density filter in the path of the beam, and the paraxial region around the main beam is photographed. The images show only the change in the main laser beam; little information about the scattered light is present. Figures 7(a) and (b) show two such photographs of the main laser beam with and without the presence of the scattering phenomenon. The central dark region between the split portions of the beam in figure 7(b) corresponds to the shadow formed by the shock. The light intensity distribution measured from the pixels along the image centerline is plotted in figure 7(c). The intensity data are normalized by the maximum value in the undisturbed laser beam. Clear splitting of the beam and spreading of light energy primarily in the downstream direction are visible in this figure. A comparison of the scales showing the spread angle in figures 6 and 7 shows that the latter corresponds to a small region close to the main beam.

A second set of images was taken to measure the intensity distribution in the wide angle streaks (figure 8). For these measurements the incident laser beam had to be brought back to its full intensity and a 12 mm wide beam stop was placed just in front of the semi-transparent screen to block the main beam. The latter was necessary to avoid blooming of the CCD elements from the intense light of the full power beam. The shadow cast by the beam stop is marked in this figure. The diffraction effects from the beam stop itself are negligible as it is placed just in

front of the screen. Once again, a comparison between the abscissa of Figures 7 and 8 shows that the entire paraxial region covered in the former falls into the shadow of the beam stop.

The intensity distribution in the long light streaks for various upstream total pressure conditions is shown in figure 8. The free-stream Mach number is kept constant at 2.0 for all of these measurements. All data are normalized by the maximum intensity value measured in the M=2.0, P_0=375KPa condition. The intensity of the scattered light is found to diminish with a drop in the free-stream total pressure, P_0. Recall that P_0 determines the jump in the refractive index across the shock. The scenario is consistent with the earlier description of shadowgraph images.

For an application of the light scattering phenomenon as a detection technique for shock, it is useful to obtain a relationship between the net scattered light and the shock strength. The latter is measured as the jump in the refractive index, Δn, across a shock. The net scattered light, I_T, is expected to be proportional to the area covered under each curve of figure 8. A plot of I_T versus Δn is shown in figure 9. All data were obtained from measurements with a fixed laser power and a fixed shock to screen distance.

The close-to-linear dependence in the semi-log plot of figure 9 shows that I_T increases almost exponentially with Δn. Unlike the shadowgraph situation, I_T is also dependent on the free-stream Mach number. However, the calculated values of I_T are not very accurate, as the scattered light from the paraxial region of beam propagation was blocked by the beam stop, and therefore, is excluded from the calculation.

The effect of the polarization of light on the wide-angle scattering phenomenon was studied by placing a polarization rotator on the path of the incident laser beam. However, within the measurement accuracy, the phenomenon is found to be independent of the light polarization.

IV. ANALYSIS

According to the laws of geometrical optics light rays are expected to bend only along the gradient of refractive index, which is along the downstream direction for a normal shock. However, clear violations are observed in the presence of the upstream fringes in the shadowgraph image, and in the upstream part of the scattered light in narrow laser beam and shock interaction. The deflection angle γ of a laser beam while crossing a shock has been calculated by Kriksunov and Pliev[11] following the paraxial ray equation, $\tan\gamma = \int_0^z \frac{dn}{d\xi} dz$, (where z is the beam propagation direction and ξ is the flow direction) and is found to be a fraction of a degree. The visible spread angle of the long streaks, on the other hand, can be as large as ±10°.

Shock waves are also known to cause light reflection. However, the reflectivity of the shock fronts is very small. Measurements by Hornig[12] showed that the optical reflectivity of a strong shock is in the order of 10^{-6}, while the present data show that the net scattered light from a narrow laser beam and shock interaction can be greater than 1% of the incident laser power. Therefore, contribution from the reflected light to the net scattered light is expected to be minimal.

The light scattering phenomenon in the two situations considered here are indicative of a strong diffraction effect. Noticeably, both phenomena appear when light disturbances travel parallel to the surface formed by a shock. In this condition a part of the beam propagates upstream and the rest downstream of the shock. The difference in the optical path length between the two parts of the beam produces phase variation. Therefore, a shock wave can be thought of as a `phase object[2]' that does little change to the magnitude of the incident light disturbance, but considerably distorts the phase. The resulting diffraction pattern can be calculated by an application of the Huygens-Fresnel principle. In an elementary way, Pfeifer *et al*[8]. used the above principle to calculate the light intensity variation caused by the passage of a normal shock in a shock tunnel. It may be worthwhile to mention that any compressible flow in general, is a phase configuration due to the variation in the refractive index with little absorption taking place, and a shock wave is the extreme case.

The present analysis is performed for the two incident light disturbance fields for which experiments were performed. At first, the ray tracing method is used to calculate the phase and intensity variation in a bundle of light rays just after crossing the shock wave. Scalar diffraction theory is applied next to calculate the irradiance distribution after the emerging rays propagate to the screen[13]. Figure 10 shows a schematic of the steps involved.

The calculation is performed in 2-dimensions and for the tip region of the bow shock. The ξ axis is along the flow direction and the z axis is along the light propagation direction. The shape of the bow shock is obtained from the shadowgraph image. A simple curve fit, $\xi = a[1-\cos(bz)]$, where a and b are adjustable constants, is found to be sufficient to analytically express the shock profile. The values of the constants for the M = 1.5 and 2.0 cases are, respectively, a= +68.62mm and +70.5mm, and b=0.0191mm^{-1} and 0.0232mm^{-1}. The refractive indices are assumed to be constant, n_u, everywhere upstream, and n_d everywhere downstream of the shock.

The ray tracing calculations start with an initial intensity distribution $\psi_0(\xi)$ from the position $z = -z_0$, away from the shock. The deflection of each ray, while crossing the shock front, is determined by an application of Snell's law. For example, at point 1 in figure 10, $\sin\delta_u/\sin\delta_d = n_d/n_u$, where δ_u is the incidence angle and δ_d is the refracted angle. After each ray emerges from the shock it is traced back to a virtual line of origin, $z = z_v$, to avoid ray crossing and also to obtain a standard reference line to start the diffraction calculation. The point of intersection of the traced back first ray, above $\xi = 0$, to its original path is used to determine z_v. The complex wave front at this virtual line of origin is determined as $\psi_1(\xi) = \alpha(\xi)\exp[i\phi(\xi)]$, where phase $\phi(\xi) = kS(\xi)$. $S(\xi)$ is the computed optical path and k is the wave number $2\pi/\lambda$; λ is the wavelength of the laser light. The amplitude $\alpha(\xi)$ is determined using conservation of energy along ray bundles. Assuming the rays do not cross, the energy between 0 to ξ_0 at the starting line should be the same as that between 0 to ξ at the virtual line of origin. This provides the integral equation

$$\int_0^{\xi_0} \psi_0 \, \psi^*_0 \, d\xi = \int_0^{\xi} \psi_1 \, \psi^*_1 \, d\xi \qquad \textbf{(2)}$$

where the superscript * represents the complex conjugate.

In the next step the calculated wave front $\psi_1(\xi)$ is propagated to the screen, z distance away from the shock, using the Fresnel diffraction equation,

$$\psi(x) = \frac{K\, e^{ikz}}{z} \int_{-\infty}^{\infty} \psi_1(\xi)\, e^{(ik/2z)(x-\xi)^2}\, d\xi, \qquad \textbf{(3)}$$

where, $\psi(x)$ is the optical disturbance on the screen and K, the `obliquity factor' = $-i/\lambda$. The complete procedure to numerically calculate the Fresnel integral is provided by Weaver[14] (see chapter 8) and will not be repeated here. In brief, it involves casting the above equation in a convolution form and applying Fourier transform and an inverse transform. The calculations use Fast Fourier Transform routines from the Numerical Recipes[15] and are performed in the same PC used for data acquisition.

Figure 11(b) shows the calculated light intensity distribution on a screen when the incident light disturbance $\psi_0(\xi)$ is assumed to consist of plane, parallel waves. This situation corresponds to the shadowgraph image of the shock. For a direct comparison, experimental data obtained from an identical condition is shown in figure 11(a). All major features, such as the central shadow and the fringe patterns upstream and downstream of the shock, are clearly captured in the numerical calculations. The width of the shock shadow in the experimental and the numerical data are nearly the same. However, the fringe spacing is slightly different and the peak intensity in the fringes is higher in the calculated data. The later is, possibly, due to an error in the experimental data, which is contaminated by high level of speckle noise. Moreover, as mentioned earlier, the experimental data were also averaged over 30 pixels.

Note that the zero on the abscissa of figure 11 represents the position of the shock, positive numbers represent downstream and negative numbers represent upstream distance. The numerical data in figure 11(b) demonstrate that the shock is located at the upstream edge of the thick shadow. This is consistent with the discussion of Merzkirch[1].

It is interesting to note an important difference between the present analysis of light scattering by shock, and the classical Fresnel diffraction by a straight edge[2]. Both problems are similar in the presence of a sudden discontinuity; however, there is an important difference between the two. The textbook treatment of diffraction by a straight edge assumes an opaque half-screen that completely absorbs the incoming light, while a shock wave does

not cause any light absorption. For the latter, transmitted light beyond the `straight edge' created by a shock produces the downstream fringes in the shadowgraph situation, and for the former, light intensity approaches zero very quickly inside the geometrical shadow of the opaque screen.

To calculate the light scattering from the narrow laser beam and shock interaction, the incident light intensity distribution is changed to that of a 2mm diameter Gaussian beam with a peak intensity of unity, $\psi_0(\xi) = \exp(-\xi^2/4)$. The beam diameter corresponds to the estimated experimental value at the shock position. Since the calculations are performed in 2-dimensions, the incident field is, in effect, a Gaussian strip of light. The calculated diffraction pattern is shown in figure 12 along with the experimental data obtained for the same condition. Once again, the primary features: splitting of the beam into two parts, strong scattering in the downstream direction and a weaker scattering in the upstream direction, are well represented. Similar to the shadowgraph situation, the experimental data also suffer from speckle noise which obliterates the weak fringes, predicted by the computational data.

The primary shortcoming of the numerical calculation is the 2-dimensional modeling of a 3-dimensional situation. The bow shock is axisymmetric; however, the present calculation assumes that the shock shape remains constant in the missing direction. A second source of error is in the assumption that the refractive index remains constant downstream of the shock. As the bow shock curves from its tip region, the fluid properties and therefore, the refractive index changes. However, the success of the numerical calculation in capturing all features of the light scattering phenomena indicates that the above concerns are of secondary importance.

V. CONCLUSION

The physical appearance of the light scattering effects in the two optical situations considered in this paper is very different. In the shadowgraph situation a wide central dark band and a few fringes are observed, while in a narrow laser beam and shock interaction situation long streaks in the far field are observed. However, a closer look reveals many similarities. First, splitting of the main laser beam in the latter can be attributed to the shock shadow formation similar to that seen in the shadowgraph situation. Second, both situations involve light propagating tangential to the shock surface. The bow shock, considered in the present work, is a three dimensional surface of revolution. In the shadowgraph image of figure 2, light has passed through every part of this surface; however, the shock shadow appears as a single line along the outer edge of the surface. Noticeably, only along this line light rays are at a grazing incidence on the shock surface; identical to the situation when long light streaks are found to appear from a narrow laser beam. Third, upstream fringes and the upstream part of the light streaks are weaker than their downstream counterparts.

Perhaps, a physical explanation unifying the two optical situations can be best provided from the Geometrical Theory of Diffraction[16,17,9]. According to this theory, electromagnetic diffraction of high frequency waves by straight edges gives rise to cylindrical diffraction edge waves. The total diffracted field, observed on the screen, is a sum of the incident waves and the edge waves. In a shadowgraph situation the spatial extent of the incident field is very large and the edge waves interfere with this field to produce the fringe patterns seen upstream and downstream of the shock. On the other hand, the use of a laser beam of narrow spatial extent separates away the edge waves which then appear as the diverging light sheet from the point of its generation. A good example is the numerically calculated scattered light pattern shown in figure 12(b). The intensity distribution shows fringe formation only in the paraxial region where light from the undisturbed beam also appears.

The effect of the refractive index jump, caused by a change in the free stream Mach number and total pressure, on the light scattering phenomena are studied in the present paper. Use of a different wavelength of light is also expected to change the scattering pattern, as in any other situation involving diffraction. A fourth parameter of interest is the thickness of the shock, which is estimated to be of the order of light wavelength[3] (light wavelength: 633 nm; shock thickness for the experimental range: 150 to 750 nm). Direct measurement of the shock thickness was not possible in the present experiment. Inclusion of this parameter in the numerical modeling requires complete solution of the Helmholtz equation. Moreover, the experimental observation, that the light scattering phenomena are independent of the polarization of the incident field, indicates that the high-frequency approximation is valid for this situation. The shock, therefore, is assumed to be of zero thickness for all analysis.

Acknowledgement
The authors acknowledge the help and valuable advice on every aspect of this paper from Dr. Richard G. Seasholtz of NASA Lewis Research Center.

Reference

[1]Merzkirch, W., *Flow Visualization*, Academic Press, (1987).
[2]Born, M. and Wolf, E., *Principles of Optics*, Sixth edition, Pergamon Press, (1989).
[3]Panda, J., "Partial Spreading of a Laser Beam Into a Light Sheet By Shock Waves And Its Use As A Shock Detection Technique," NASA CR-195329, May 1994.
[4]Panda, J., "Wide Angle Light Scattering in Shock-Laser Interaction," *AIAA J.*, **34**, No. 3, (Mar. 1996).
[5]Panda, J., "Shock Detection Technique Based On Light Scattering by Shock," *AIAA J.*, **34**, No. 3, (Mar. 1996).
[6]Waltham, J. A., Cunningham, P. F., Michaelis, R. N., Campbell, R. N. and Notcutt, M., "The Application of the Refractive Fringe Diagnostic to Shocks in Air," *Optics and Laser Technology*, **19**, No. 4, pp. 203-208, (Aug. 1987).
[7]Vasil'ev, L. A., *Schlieren Methods*, Israel Program For Scientific Translations, (1971).
[8]Pfeifer, H. J., Vom Stein, H. D. and Koch, B., "Mathematical and Experimental Analysis of Light Diffraction on Plane Shock Waves," Proc. Int. Cong. High-Speed Photography, 9th, pp. 423-426, 1970.
[9]Langois, P., Lessard, R. A. and Boivin, A., "Real-Time Curvature Radii Measurements Using Diffraction Edge Waves," *Applied Optics*, **24**, No. 8, pp 1107-1112, (1985).
[10]Davis, D. O., Hingst, W. R. and Bodner, J., "Flow Coefficient Behavior For Isolated Normal And 20 Degree Boundary-Layer Bleed Holes," NASA TM-106816, 1994.
[11]Kriksunov, L. Z. and Pliev, A. E., "Refraction of Laser Beams at a Compression Shock," *Sov. J. Opt. Technology*, Vol. 51, No. 7, July 1984. English Translation by The Optical Soc. of America, 1985.
[12]Hornig, D. F., "Shock Front Measurements by Light Reflectivity," in *Physical Measurements in Gas Dynamics and Combustion*, ed. R. W. Ladenburg, Princeton University Press, pp. 203-210, (1954).
[13]Lewis, W. L., Teets, R. E., Sell, J. A. and Seder, T. A., "Temperature Measurements in a Laser-Heated Gas by Quantitative Shadowgraphy," *Applied Optics*, **26**, no. 17, pp.3695-3704, (1987).
[14]Weaver, H. J., *Applications of Discrete and Continuous Fourier Analysis*, John Wiley & Sons, (1983).
[15]Press, W.H., Flannery, B. P., Tuekolsky, S.A. and Vetterling, W. T., *Numerical Recipes, The Art of Scientific Computing*, Cambridge University Press, (1986).
[16]Keller, J. B., "Geometrical Theory of Diffraction," *J. Opt. Soc. Am.*, **52**, pp. 116, (1962).
[17]Kouyoumjian, R. G., "The Geometrical Theory of Diffraction and its Application," in *Numerical and Asymptotic Techniques in Electromagnetics*, R. Mittra, Ed. (Springer, New York), pp. 165-215, (1975).

Table I. Shock Properties Relevant To The Light Scattering Phenomenon

Mach No. M		free stream total Pressure P_0, KPa	Air Density Kg/m^3		Refractive Index		
Upstrm	Downstrm		Upstrm	Downstrm	Up, n_u	Dn, n_d	Diff., Δn
1.5	0.70	237	1.115	2.076	1.000252	1.000468	0.000217
		168	0.791	1.473	1.000178	1.000332	0.000154
		134	0.629	1.171	1.000142	1.000264	0.000122
2.0	0.58	375	1.027	2.738	1.000232	1.000618	0.000386
		306	0.838	2.235	1.000189	1.000504	0.000315
		237	0.649	1.732	1.000147	1.000391	0.000244
		168	0.461	1.228	1.000104	1.000277	0.000173
		134	0.366	0.976	1.000083	1.000220	0.000138
2.5	0.51	375	0.588	1.959	1.000133	1.000442	0.000309
		341	0.534	1.779	1.00012	1.000401	0.000281
		306	0.48	1.6	1.000108	1.000361	0.000253
		272	0.426	1.419	1.000096	1.000320	0.000224
		237	0.372	1.239	1.000084	1.000280	0.000196
		168	0.264	0.879	1.000059	1.000198	0.000139

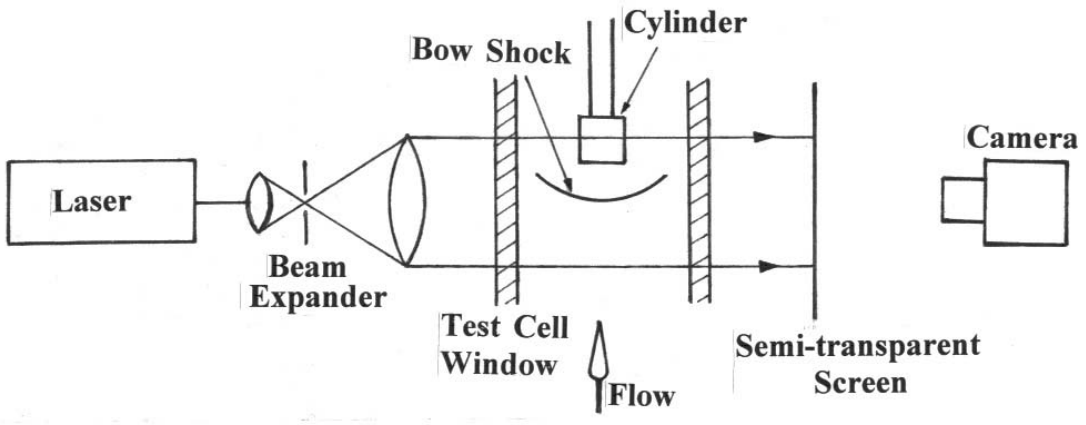

Fig. 1. Schematic of shadowgraph arrangement.

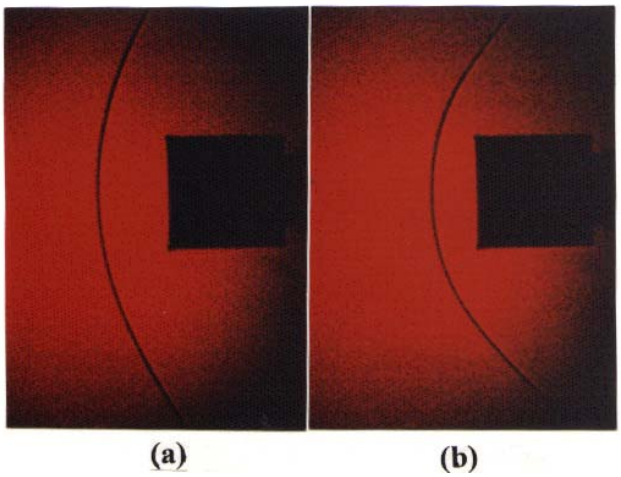

Fig. 2. Shadowgraph image of the bow shock formed ahead of bluff cylindrical body; (a) M = 1.5 and (b) M = 2.0

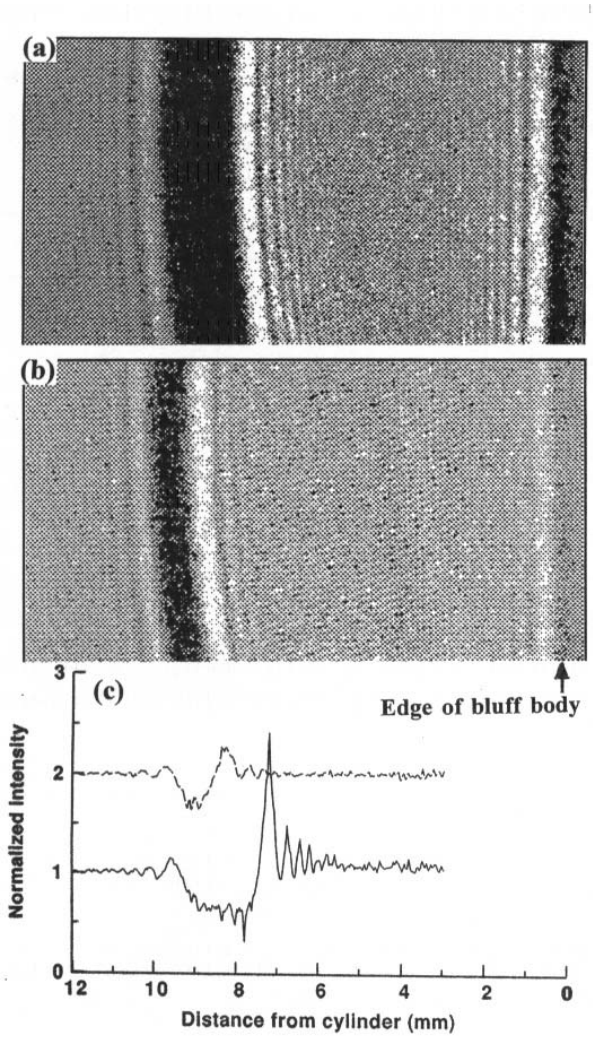

Fig. 3. (a), (b) Enlarged view of the tip region of the bow shock obtained with a CCD camera; M=1.5 and P_0=237 and 134KPa, respectively. (c) Light intensity distribution along centerline, ____ P_0=237KPa and P_0=134KPa. The latter is shifted by one major division.

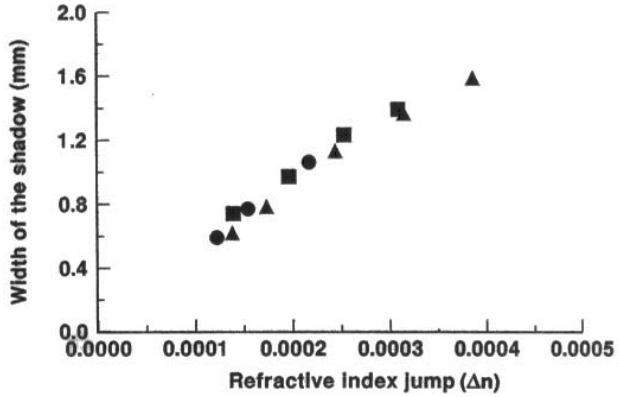

Fig. 4. Width of the central dark band in shadowgraph image of shock versus the refractive index difference created across the shock; • • , M=1.5; ⮝ ⮝ , M=2.0; ▪ ▪ , M=2.5.

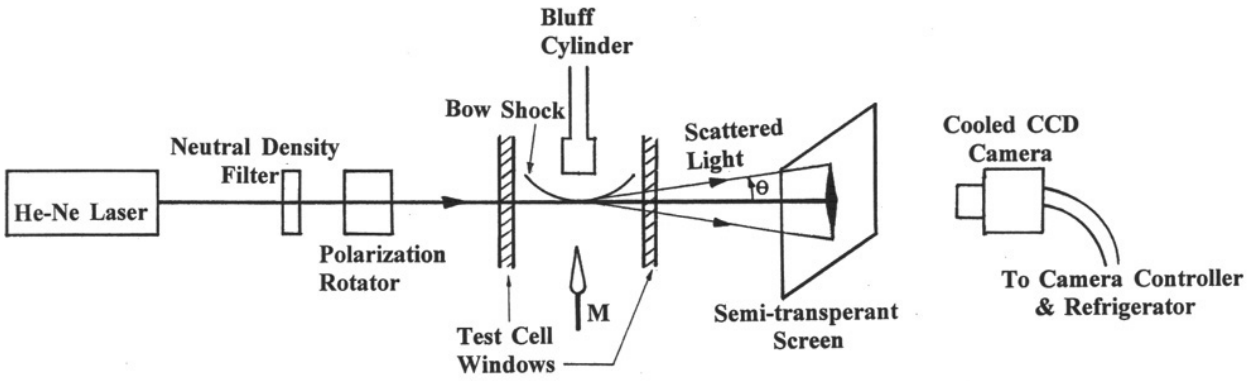

Fig. 5. Schematic of the arrangement to visualize and measure the wide angle light scattering phenomenon.

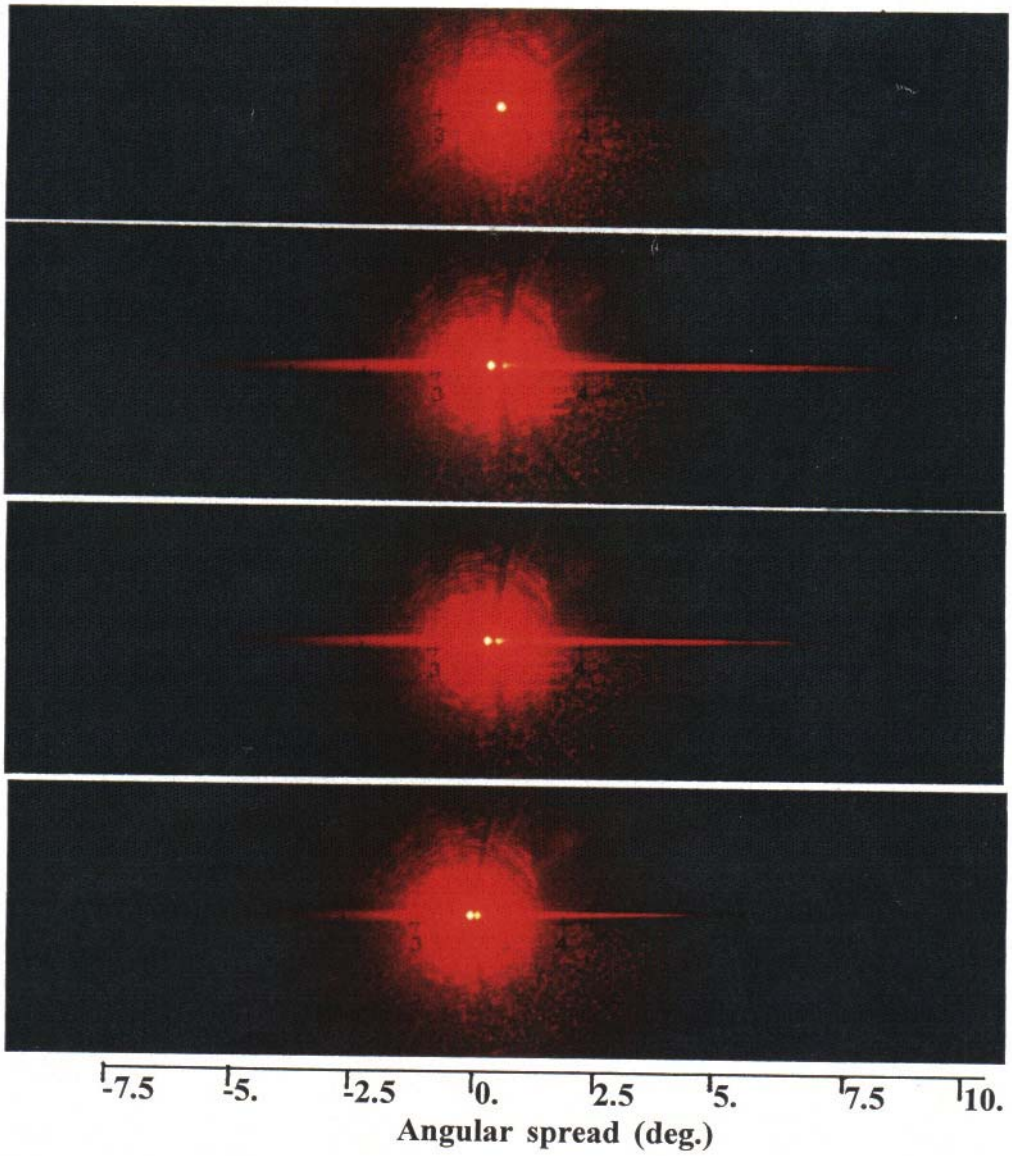

Fig. 6. Cross-sectional views of the laser beam showing the wide angle light scattering; (a) No flow; (b), (c), (d) interaction with shocks formed in M=2.0 flow and P_0=306, 237 and 168KPa, respectively.

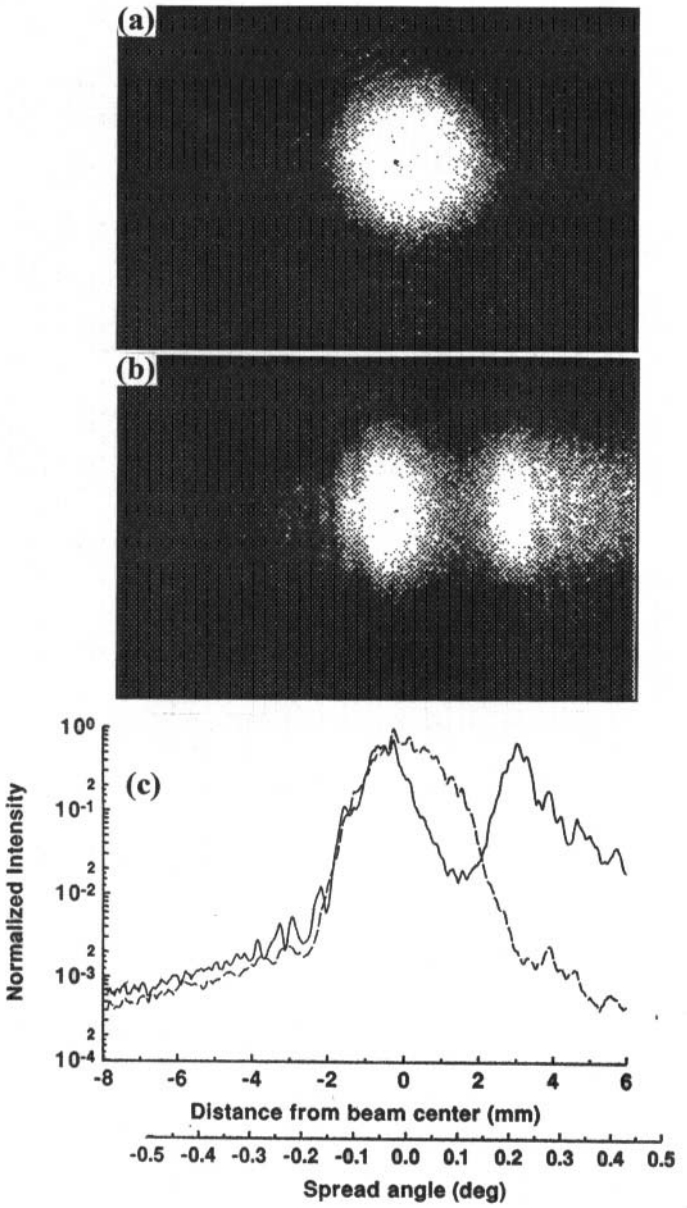

Fig. 7. Enlarged view of the main laser beam; (a) no-flow; (b) interaction with a shock in M=2 and P_0=237KPa flow. (c) light intensity distribution along centerline;_ _ _,no-flow; ____ M=2.0, P_0=237KPa.

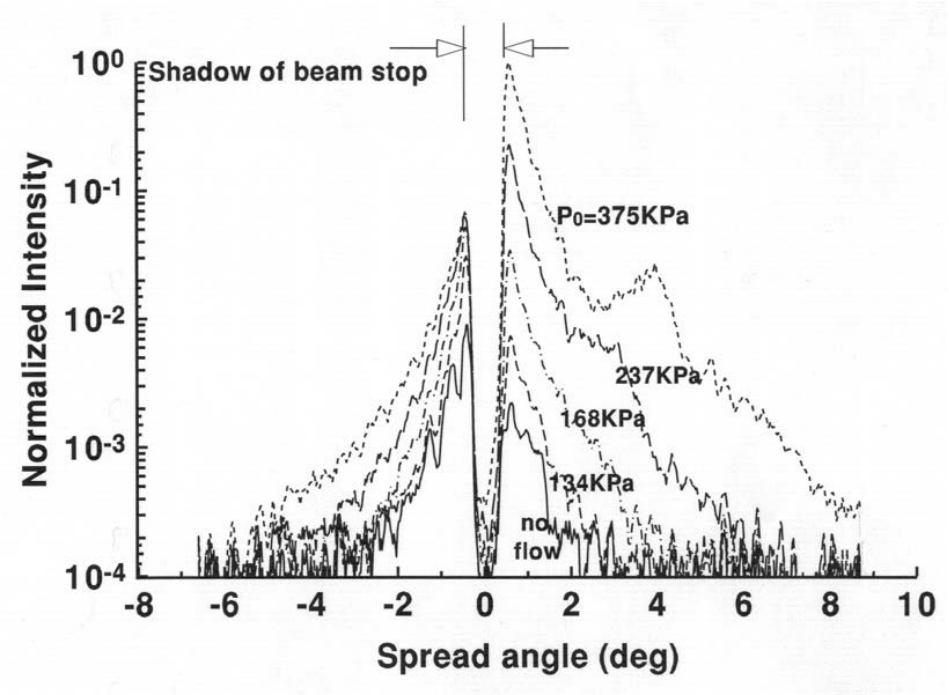

Fig. 8. Intensity distribution in the scattered light from interaction with shocks formed in M=2.0 flow. Shock to screen distance = 292mm.

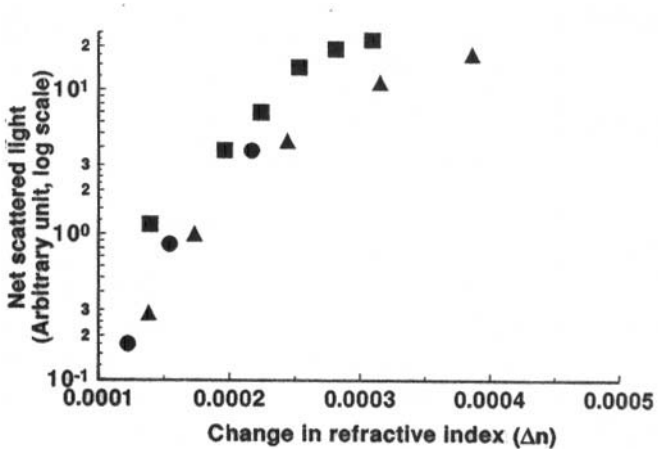

Fig. 9. Net scattered light in narrow laser beam and shock interaction versus the refractive index jump across the shock; • •, M=1.5; ▲ ▲, M=2.0; ▪ ▪, M=2.5.

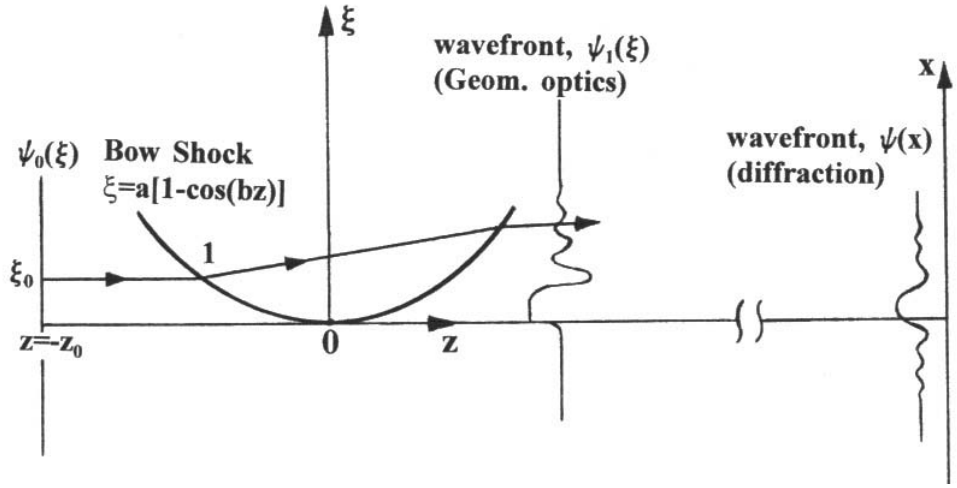

Fig. 10. Schematic of the procedure to calculate light scattering by shock.

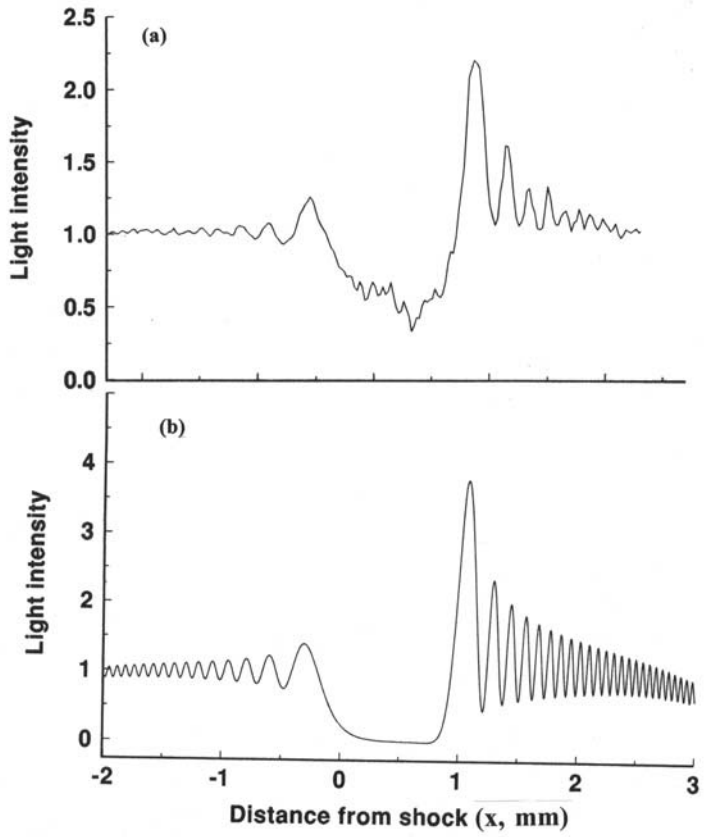

Fig. 11. A comparison between (a) experimental and (b) calculated intensity distribution in the shadowgraph image of shock; M=2.0, P_0=237KPa, shock to screen distance = 216mm.

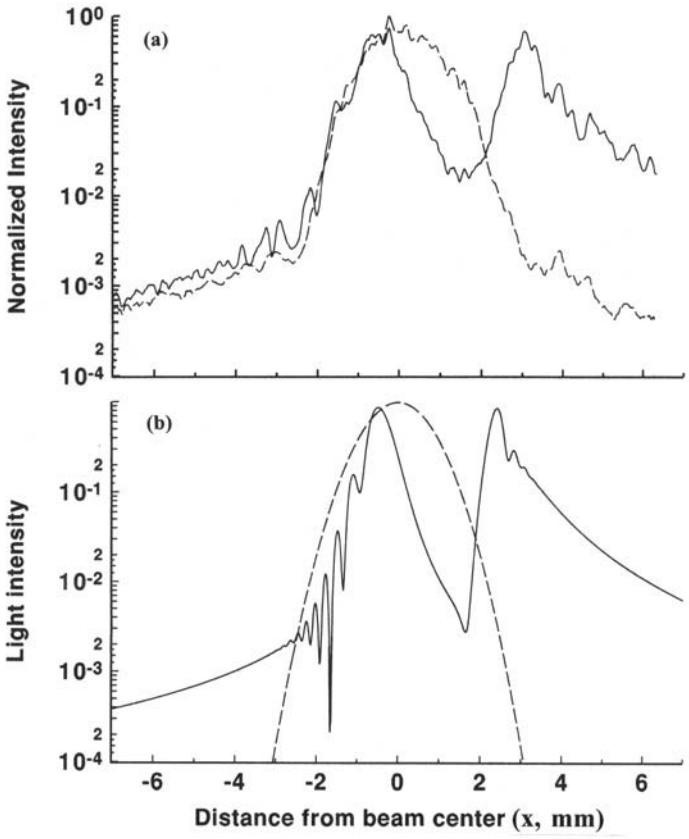

Fig. 12. A comparison between (a) experimental and (b) calculated intensity distribution in the narrow laser beam and shock interaction; M=2.0, P_0=237KPa, shock to screen distance = 737mm; _ _ _ undisturbed beam; ___after interaction with shock.